Metamaterial Antenna Designs for a 5.8-GHz Doppler Radar

Hasan Önder Yılmaz and Fatih Yaman

***Abstract*— The aim of this paper is to investigate applicability and the effectiveness of the metamaterial-based antennas for a 5.8-GHz Doppler radar. Thus, a double negative index metamaterial structure is designed as a transmitter antenna and a near-zero index medium is integrated with a patch antenna for the receiver. Significant improvements in bandwidth for the transmitter, slight improvements in gain and in directivity for the receiver, and typically size reduction for both antennas are obtained. It is shown that return loss, radiation pattern, and gain measurement results of the newly designed antennas agree well with the simulations for a desired frequency band. The last part of the study is devoted to express the adaptation of the antennas for a low-power radar system whose aim is to reconstruct the velocity of the human, indoor as well as behind the wall, from the shift in the received frequency. The accuracy of the velocity measurements and field test results of the radar with the metamaterial antennas are reported.**

***Index Terms*— Antenna, double negative index, metamaterial, near-zero index, short-range Doppler radar.**

I. Introduction

COMPACT and low-cost short range Doppler radar systems are capable of detecting mobile targets by consuming less energy both in outdoor and indoor applications, [1], such as police radar, through-wall vital sign recognition and autonomous devices [2]–[5]. Accordingly, we propose a bi-static metamaterial antenna concept to improve radar transmitter antenna size and weight, range, and overall efficiency at 5.8 GHz. In this way, we could avoid certain disadvantages of using microstrip antennas: e.g., to increase the directivity, one has to increase the number of patches in the microstrip array antenna; to obtain high gain, one has to increase the height of the dielectric substrate (see [6]). Both requirements make the structure bulky and cause extra power loss on the receiver antenna. On the other hand, metamaterials, which are defined as artificially engineered structures, exhibit anomalous values for negative relative permittivity/permeability, ($\epsilon_r, \mu_r \leq 1$), and gained attention for optical and microwave applications in the last decade (see [7]–[11]). Particularly, novel antenna designs based on metamaterials played important roles in practice since their performance was significantly improved. A large amount of antenna studies, which we could mention only a few of them in here, have been published with the boom of metamaterials researches at the beginning of the year 2000 [12]–[16]. Among them, [12]–[14] use a metamaterial epsilon near-zero material slab to confine the radiated power in a narrow angle under necessary conditions. In addition, in [15], it is shown that the zero-index material, which is placed over a typical patch antenna, could increase the gain. Left-handed characteristics and the considered negative index metamaterial medium's remarkable impact on the antenna parameters in terms of significant broadening of the bandwidth, low loss, reduction in the dimensions, and low voltage standing wave ratio values were demonstrated by Li *et al.* [16].

Existence of negative (ϵ and μ) left-handed/metamaterials is explained theoretically by Veselago [18]. Afterward, it is shown that aligning metallic wires along the propagation of wave yields negative permittivity and appropriately designed conducting split rings with its axis along the direction of propagation represents negative permeability, in [19] and [20], respectively. We note that even though the negative permittivity can be observed in ferroelectrics and plasma, the negative permeability does not exist in nature. Smith *et al.* [21] expressed the behavior of double negative medium, i.e., both permittivity and permeability negative at a certain frequency, where the study led to a large amount of metamaterials to be involved in the research and developments in the field of sensors, filters, and antennas in the microwave region. Furthermore, Pendry *et al.* [19] showed that the tunable low frequency of plasma at a dielectric–conductor boundary can be a wide research area for RF engineers. In this context, Enoch *et al.* [12] used a media having optical index close to zero and demonstrated that an array of metallic–dielectric boundary composite material can reshape the radiation pattern of embedded electromagnetic wave source. More recent studies, see [13]–[15], on planar 2-D structures illustrated that highly directive antennas can be designed by using near-zero epsilon metamaterials without arraying the patches.

Within this framework, the main motivation of this paper is to utilize the mentioned advantages of the metamaterials for antenna design in order to improve the short-range Doppler radar characteristics. The Friis transmission equation implies that the maximum range of a radar can be increased with the antennas having larger gains (see [22]). Along this line, for the

Manuscript received October 12, 2018; revised April 8, 2019; accepted April 13, 2019. Date of publication May 1, 2019; date of current version March 10, 2020. This work was supported by the Izmir Institute of Technology Scientific Research Program (BAP) under Grant 2017IYTE44. The Associate Editor coordinating the review process was Huang-Chen Lee. *(Corresponding author: Fatih Yaman.)*

The authors are with the Department of Electrical and Electronics Engineering, Izmir Institute of Technology, Izmir 35430, Turkey (e-mail: fatihyaman@iyte.edu.tr).

Color versions of one or more of the figures in this article are available online at http://ieeexplore.ieee.org.

Digital Object Identifier 10.1109/TIM.2019.2914131

transmitter, a double negative index metamaterial antenna is implemented due to its wide bandwidth (3.5–8.0 GHz) and low-level side/back lobes in the radiation pattern. And for the receiver stage, a highly directive near-zero epsilon metamaterial supported antenna having a high gain and a narrow beamwidth is designed to increase the radar range and the resolution of the targets in the angular detection. The investigated radar system additionally consists of a microstrip power divider and coaxial SubMiniature version A (SMA) connectorized components, such as a voltage controlled oscillator (VCO), a mixer, microwave power amplifiers, and attenuators, so that we could build a compact and low-cost setup.

The organization of this paper is as follows. Section II is devoted to illustrate the design of the double negative index transmitter antenna and the related literature. Afterward, the receiver antenna is explained in detail. Integration of antennas to the Doppler radar is described in Section IV. We summarize our results and findings in the latest part of this paper. Note that the idea of this paper is given by Yılmaz and Yaman [7]. In this paper, we discuss the study thoroughly and present extensive investigations, comparison results of simulations and measurements, new experiments, and related observations.

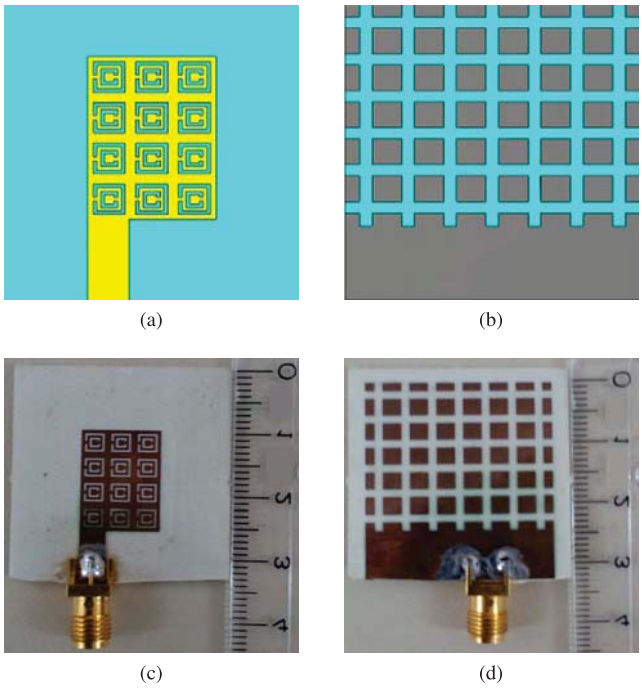

Fig. 1. Simulated and realized transmitter (Tx) antenna. (a) Top view (simulation). (b) Bottom view (simulation). (c) Top view (realized). (d) bottom view (realized).

II. Tx: Double Negative Index Antenna

This section is devoted to explain the fundamental reasons of choosing a double negative index antenna as a transmitter, to describe the detailed design procedure, the geometry, and the dimensions of the structure, and to illustrate comparisons for the simulation and the measurement results obtained for the return loss and 2-D radiation patterns.

Microstrip patch antennas are popular in practice due to their low-cost, lightweight, and simple fabrication techniques. However, in order to improve their bandwidth, size, efficiency, and directivity, one has to optimize tradeoffs between desired parameters and structure of the antennas. For instance, the bandwidth of the antenna can be increased by using a thicker substrate, which may increase the power loss as well. Besides, microstrip patch antennas generally have a strong unwanted radiation in the vertical direction according to the patch plane due to surface waves such as lateral and leaky waves (see [16]). As a remedy for the above-mentioned points, we propose to use a metamaterial-based transmitter antenna in our application. Therefore, we can significantly improve the radiation efficiency in the horizontal direction and can reduce the size of the antenna. Furthermore, broad bandwidth characteristic of the antenna simplifies the impedance matching.

In the double negative index antenna designs, arrays of specific structures are mounted on top of a dielectric substrate to represent a negative permittivity, and grid patterns are employed for the bottom of the substrate to demonstrate a negative permeability behavior. We use arrays of complementary split ring resonator (CSRR) on the top layer, see Fig. 1(a) and (c), instead of a microtriangle that was presented in [16]. CSRRs are well-known structures such that they can be obtained by etching conducting patches. For the bottom ground plane, periodically distributed cross-strip line gaps are designed to obtain negative permeability at the desired frequency range [see Fig. 1(b) and (d)].

The equivalent model of the proposed antenna can be considered as a combination LC ladder resonant circuits, see the Appendix, see Fig. 16, such that the analysis is analogous to periodic filter-type structures, [17], [26]. The array of CSRRs provides a passband in the higher frequency band, whereas the second passband occurs in the lower frequencies due to proposed grid configuration. To adjust passband for the desired frequency, we optimize the double negative index antenna parameters such that two different passbands coincide at 5.8 GHz. We note that the structure induces a backward wave that can travel along the plane of the patch. Further information on the electromagnetic properties and equivalent circuits of CSRR and cross strip-line structures can be found in [23]–[27].

We were inspired by the studies [16], [33] in the design of the transmitter antenna. First, a typical single patch dimension 14.24 mm × 18.28 mm is calculated analytically from the reference study given in [22]. Afterward, a single complementary split resonator (CSRR), which is the reversed structure of squared split ring resonator (SSR), is constructed. Initial CSRR parameters, $w = s = 0.3$ mm, $g = 0.2$ mm, edge length $= 3.4$ mm, are obtained using the calculated values for SSR presented in [33, Table I]. The following step is finding the sufficient integer number of CSRRs which could fit on the patch area. Therefore, we located 12 split ring resonators on the of the substrate instead of the single patch. A grid structure is designed for the bottom part of the antenna. The length of a squared patch $a = 3.6$ mm and the distance between two of them $r = 0.4$ mm are chosen as given in [16] such that the effective permeability shows negative values

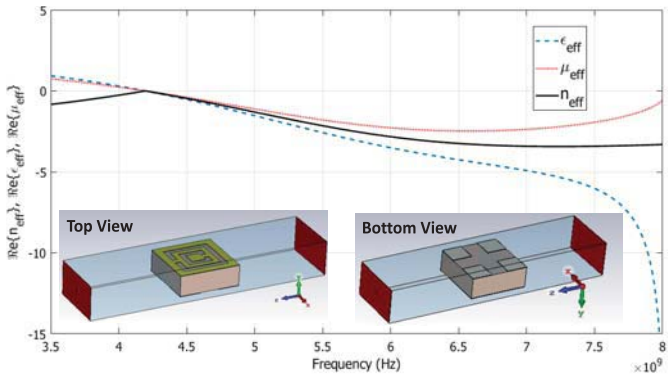

Fig. 2. Real values of effective permittivity, effective permeability, and refractive index variation of the proposed negative index metamaterial with respect to frequency.

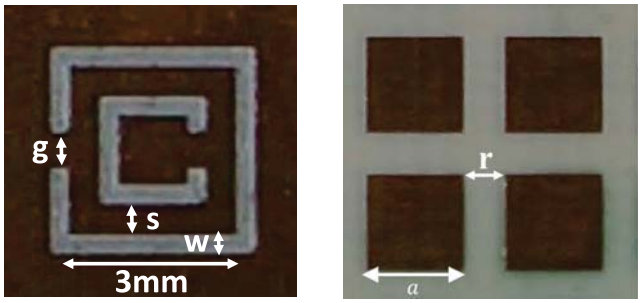

(a) (b)

Fig. 3. Dimensions for the realized transmitter antenna ($w = s = 0.35$ mm, $g = 0.4$ mm, $a = 2.8$ mm, $r = 1.2$ mm). (a) Single CSRR. (b) Grid structure.

according to the theory in [19]. Hence, we could find the number of squared patches which can be distributed on the bottom. Finally, the dimensions of geometrical configurations and location of the feeding line are chosen for the required antenna performance at 5.8-GHz via CST-Microwave Studio (MWS) electromagnetic simulator [28], for our substrate parameters permittivity and height.

Fig. 2 illustrates the double negative index behavior of the single optimized double negative index element. For the simulations, we follow the procedure given in [34] and [35] and locate the structure in a waveguide. Perfect magnetic boundary condition (PMC) is applied at the faces along the axis of the ring $\pm x$, and perfect electric conductor condition (PEC) is used at the walls $\pm y$ in Fig. 2. The structure is excited such that the incident TEM wave propagates along the z-axis. Furthermore, we added vacuum regions between the top and bottom portions of the CSRR and the waveguide walls to avoid unwanted contacts. By using the so-called retrieval method, see [35]–[38] for details, the constitutive parameters of the proposed medium are negatively obtained in the desired frequency and the effective refractive index value is found as $n_{\text{eff}} \approx -2.58$.

For the antenna design, 12 split ring resonators [size of the resonators is shown in Fig. 3(a)] and the corresponding feedline are located on the upper layer of the structure, whereas a grid structure having 30 small grounding squares [four of them can be seen in Fig. 3(b)] is located on the bottom side. The substrate is chosen as Roger 4730 as low-loss

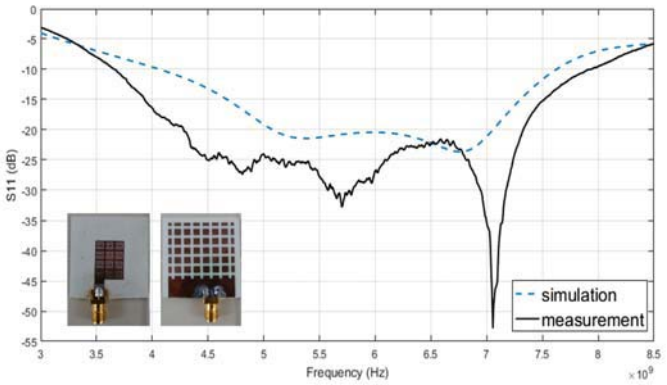

Fig. 4. S_{11} versus frequency for Tx antenna.

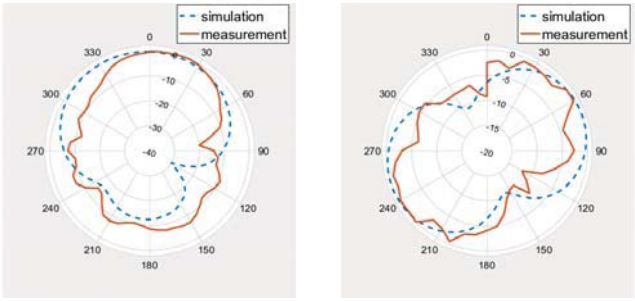

(a) (b)

Fig. 5. 2-D normalized radiation patterns for Tx antenna at 5.8 GHz. (a) Copolarization H-plane. (b) Copolarization E-plane.

dielectric with relative permittivity of $\epsilon_r = 3.00 \pm 0.05$ and thickness of 1.52 mm. The area of the mounted upper patch is 12 mm × 16 mm. Measurements are performed through a vector network analyzer in an anechoic chamber to eliminate possible unwanted reflections from the environment.

It can be seen from the return loss, Fig. 4, that the bandwidth below -10 dB cutoff is slightly larger for measurement when compared to the simulation. The difference between the measurement and the simulation is related to the fabrication tolerance for the complicated CSRR patterns such that it decreases especially in the neighborhood of the 5.8-GHz operating frequency and reaches below -20 dB in the considered bandwidth. Therefore, one can conclude from Fig. 4 that the reflected waves are minimized at the antenna connection point at a frequency of 5–7 GHz and the signal from the oscillator is efficiently radiated to the space.

Simulated and measured 2-D radiation patterns for horizontal and vertical polarizations, which are given in Fig. 5, show that the designed structure behaves as a traveling wave antenna due to backward wave propagation along the horizontal plane as a consequence of using a left-handed medium. Hence, the radiation occurs in the horizontal direction, which plays the main role in our radar application. According to Fig. 5(a), the pattern obtained from the simulation is less directive and the 3-dB beamwidth is higher $\approx 90°$, whereas the measured one is more directive and the 3-dB beamwidth is $\approx 60°$. Furthermore, the gain of the transmitter is obtained as 6.5 dB at 5.8 GHz. Interestingly, we obtained more consistent variations of simulations and measurements for the vertical polarization [see Fig. 5(b)].

III. Rx: Near-Zero Epsilon Metamaterial Antenna

In order to maximize the range and to obtain angular localization, a pencil-beam, with high gain and directivity, is required for the receiver antenna. Therefore, the so-called quasi-monostatic configuration via the near-zero epsilon metamaterial antenna is preferred for the Doppler radar in this study.

The idea of Pendry *et al.* [19] on modeling low-frequency plasmon with metallic wire lattice in dielectrics received big attention in highly directive antenna studies for microwave applications. In this context, such structures are designed using a periodic mesh of metallic thin wires whose dimensions are smaller than the operating wavelength. Here, although a thin plate-type structure is implemented instead of a volumetric one, the principles and the idea presented in [19] and the implementation method in [15] are followed. Note that the vertical wires, which we omit in the fabrication, have a negligible effect on the radiation direction of the patch antenna (see [12]). Accordingly, a near-zero index slab consisting of three layers is designed, whose aim is to confine the radiated beam in a narrow angle in the direction of the antenna plane's normal vector, unlike the typical patch antenna radiation pattern. Both sides of the substrate have the dual pattern of the transmitter's bottom side grid configuration, which means that the squared geometries are chosen as dielectrics and the lines are conductors for the receiver. The substrate with the identical grid configuration of each side corresponds to a single layer.

Pendry *et al.* [19] presented that plasma frequency of such a mesostructure is given as follows:

$$\omega_p^2 = \frac{n_{\text{eff}} e^2}{\epsilon_0 \mu_{\text{eff}}} = \frac{2\pi c_0^2}{\ell^2 \ln(\ell/\rho)} \tag{1}$$

where ρ is the width of conductor, ℓ is the gap between them (lattice constant), ϵ_0 is the free space permittivity, ω_p is the plasma frequency, and ω is the frequency of the excited electromagnetic wave.

In microwave frequencies, the effective permittivity ϵ_{eff}

$$\epsilon_{\text{eff}} = 1 - \frac{\omega_p^2}{\omega\left(\omega + i\epsilon_0 \ell^2 \omega_p^2/\pi\right)\rho^2 \sigma} \tag{2}$$

where σ is the conductivity of the metal, and the propagation constant K

$$K = \omega \frac{\sqrt{\epsilon_{\text{eff}}}}{c_0} = \frac{\sqrt{\omega^2 - \omega_p^2}}{c_0} \tag{3}$$

can be defined according to the rigorous homogenization theory. According to (2), the effective permittivity can be negative when the frequency is below ω_p. In another interesting case, effective permittivity can be $\epsilon_{\text{eff}} < 1$ when the frequency is just above the plasma frequency, which means that the effective index can be close to zero. For small optical index values of the slab, the radiated field focuses in the vicinity of the normal vector to the surface. Therefore, the improvement of the directivity and a narrow beamwidth could be achieved.

In this framework, initial values for $\rho = 1.5$ mm, and $\ell = 16$ mm, in (1) are calculated as given in [15].

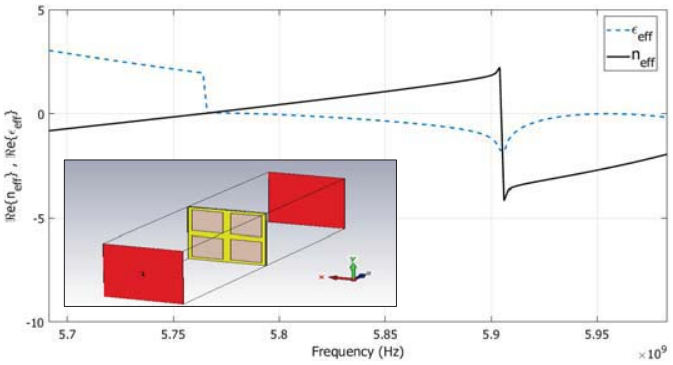

Fig. 6. Effective permittivity and refractive index variation of near-zero index metamaterial with respect to frequency of interest.

Then, we construct a square grid with four elements on both sides of the substrate. To test whether the value of the permittivity is near zero at the operating frequency, we locate the structure in a waveguide. Therefore, we could obtain effective permittivity using the retrieval method and observe the demanded behavior as shown in Fig. 6.

Afterward, a standard patch antenna with the parasitic elements is designed for the near-zero index slab to use both structures as a directive receiver considering the analogy for an antenna with its reflector. We refer [6], [15], and [22] for a detailed information on the patch antenna design. The slab is located at a certain distance in the near field region over the patch where the optimum distance is obtained by trial and error via parametric simulations. The electromagnetic simulations of the combined structure via CST-MWS showed that the number of elements on the layer has to be increased up to 25 and at least three layers should be used in order to obtain the required parameters. Impedance matching due to the coupling between near-zero mask and microstrip line feeding of the patch has taken into account. The substrate of the patch antenna and the near-zero index slab is Roger 4730JXR ($\epsilon_r = 3.00$) with 1.52 mm thickness. The patch antenna is loaded by parasitic components in order to increase the bandwidth by 13.94 mm × 4.02 mm.

Dimensions of the patch, parasitics, and near-zero index slab of the designed antenna are indicated in Fig. 7. A foam layer with the 19 mm-thickness is located between the patch and metamaterial layers and fixed with plastic stripes in the realized structure.

The return loss behavior of the designed patch receiver antenna shown in Fig. 8 is determined by a vector network analyzer in the laboratory. The most probable reason of the appearance of a second resonance in the measurement is due to a small misalignment for one or more near-zero index layers. However, the gain, using the three-antenna method, and radiation pattern experiments are performed in the anechoic chamber [see Figs. 9 and 10(a) and (b) for the above-mentioned results].

In general, good agreements between simulation and measurements are obtained. Especially, the consistent variation in the return loss curves below −10 dB is noticeable in Fig. 8. An efficient resonance, which corresponds return loss lower than −30 dB so that the radar can operate in the

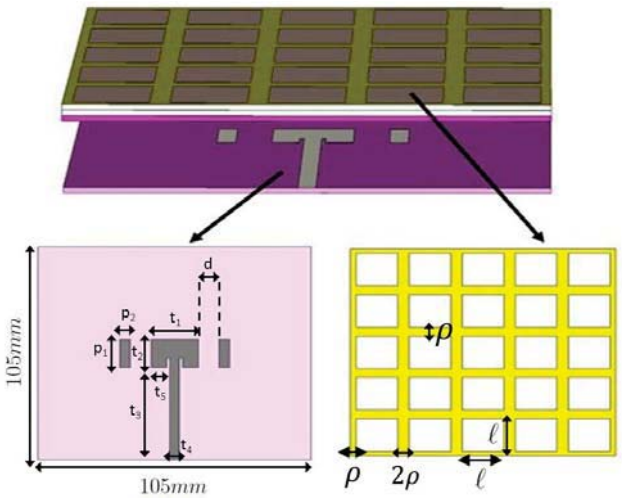

Fig. 7. Simulated receiver (Rx) antenna ($p_1 = 13.96$ mm, $p_2 = 4.02$ mm, $t_1 = 17.96$ mm, $t_2 = 13.96$ mm, $t_3 = 45.73$ mm, $t_4 = 3.87$ mm, and $t_5 = 7.98$ mm, d = 8 mm, $\rho = 2.2$ mm, and $\ell = 16.6$ mm).

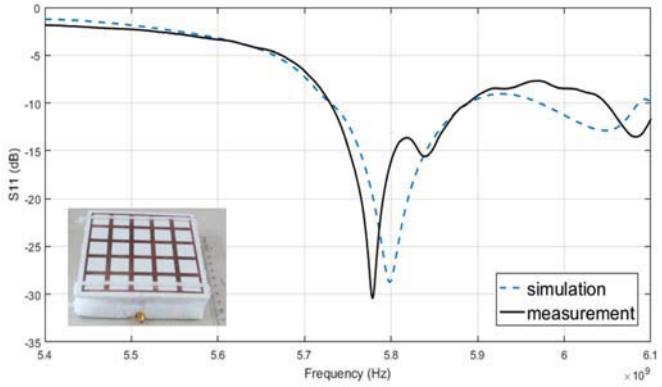

Fig. 8. S_{11} versus frequency for Rx antenna.

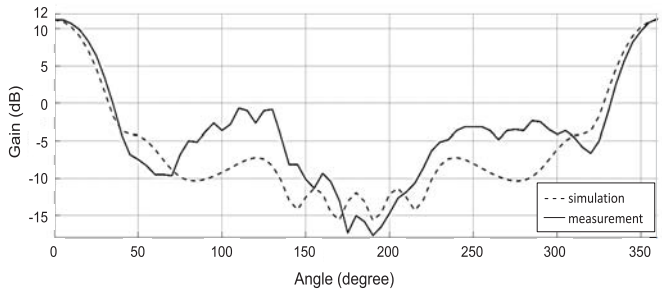

Fig. 9. Gain versus angular degree for Rx antenna.

frequency band 5.78–5.8 GHz, occurs in 5.72–5.82 GHz and in 5.75–5.85 GHz according to simulation and measurement, respectively. Similarly, 3-dB beamwidth and gain values are obtained as (33°, 11.34 dB) in simulation and (32°, 11.33 dB) in measurement.

Horizontal and vertical polarization (normalized) radiation patterns of the designed receiver antenna are shown in Fig. 10(a) and (b). As it can be seen from these figures, the simulation and measurement results agree more in horizontal polarization when compared to vertical polarization where the noise effect can be more clearly seen in vertical polarization due to low received power.

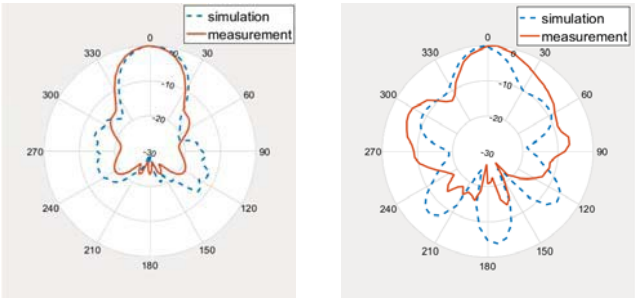

(a) (b)

Fig. 10. 2-D normalized radiation patterns for Rx antenna at 5.8 GHz. (a) Copolarization H-plane. (b) Copolarization E-plane.

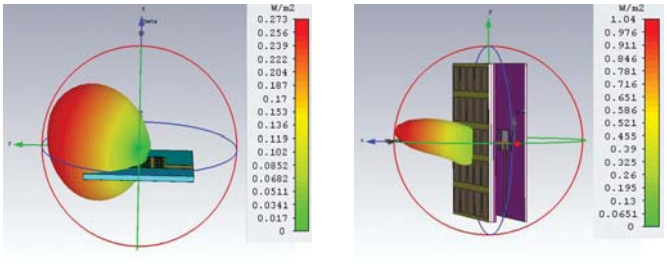

(a) (b)

Fig. 11. 3-D radiation patterns of Tx and Rx antennas. (a) Transmitter antenna. (b) Receiver antenna.

IV. Integration of the Tx and Rx Antennas on a Short-Range Doppler Radar

After realization and measurements of the Tx/Rx antennas, a low-profile short-range radar system is built. Fig. 11 is prepared to illustrate 3-D far-field power patterns of the Tx and Rx antennas, where the orientation of each antenna with respect to the radiated power distribution is described. With the help of these plots, one can decide the mounting directions of the antennas on the radar.

The system setup of the Doppler radar, which is used as a test bench for the proposed antennas, is shown in Fig. 12. Furthermore, the types and product identification numbers of the SMA connectorized components, such as VCO, mixer, amplifiers, and attenuators from Mini-Circuits Inc., are listed. Here, we note that a microstrip 3-dB Wilkinson power divider is also realized for 5.8-GHz system operation. For detailed information on the splitter design, we refer [31].

During the radar operation, an amplified continuous wave (CW) is applied to the transmitter stage and to the mixer. The echo signal carrying the Doppler shift is multiplied with the reference signal from the signal source in order to obtain only its frequency-shifted portion. Afterward, the resultant signal is filtered, amplified, and processed via a computer. The output is displayed using a radar interface which is an open source code [32].

We first check the accuracy of our velocity measurements for a small target (conducting ball with a diameter of 7 cm) with a small radar cross section (RCS) for low velocities by realizing the well-known pendulum experiment. The radar is located approximately 4 m far from the target, and the conducting ball is left for free fall from 85 cm height.

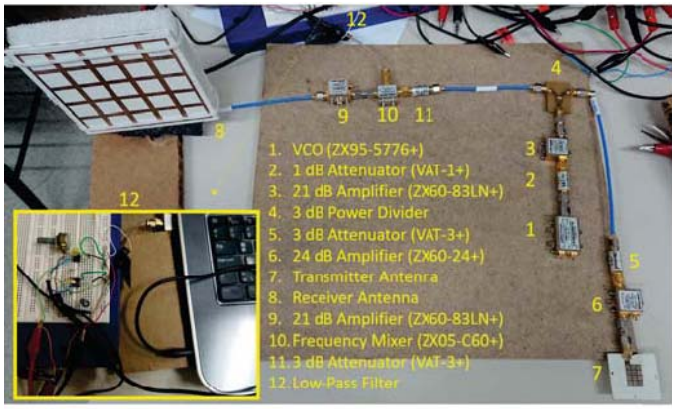

Fig. 12. Short-range Doppler radar system with metamaterial antennas.

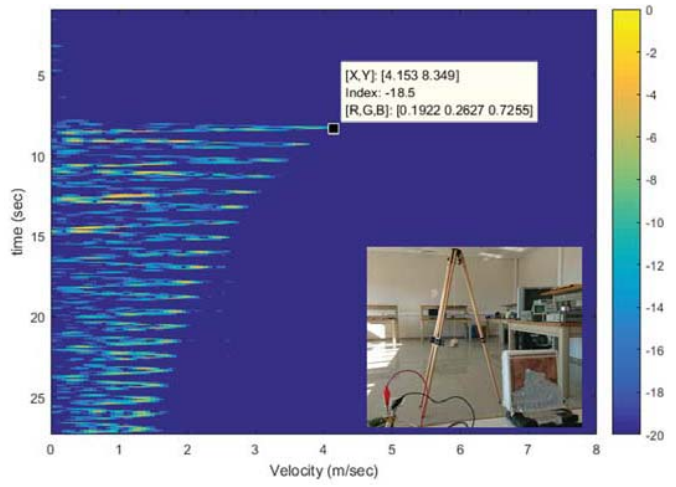

Fig. 13. Doppler experiment setup and the measurement data of a conducting ball left for a free-fall in (m/s) and received signal amplitude (colorbar in dB).

The maximum velocity of the ball is analytically calculated as 4.08 m/s. According to the measured data, the maximum velocity of the ball is read as 4.15 m/s and the periodic behavior of the swinging is clearly observed in Fig. 13.

The second experiment is devoted to through-wall operation, hence the system is placed 4 m far from an ordinary concrete wall. In this scenario, an average tall man can run and walk in the range of 4–6 m behind the wall. These series of actions are performed six times and between movements ≈5 s pauses are also seen from Fig. 14.

We additionally performed the preliminary field tests of the radar system with the car. We used a similar test setup as presented in [39] for cantennas. In an experiment [40] with the metamaterial antennas, the first radar signal is observed after 4 s of data recording when the car is ≈72.5 m away from the system with 44 km/h actual speed, see the corresponding 12 m/s-velocity measurement data in Fig. 15. Afterward, the car is decelerated toward the radar such that the increase in the received signal amplitude can be observed clearly in the latest seconds of the action.

In our experiments, we observed the applicability of the metamaterial antenna concept in a Doppler radar and obtained a relatively large radar range due to high gain values of the antennas. Furthermore, the Rx antenna with a narrow

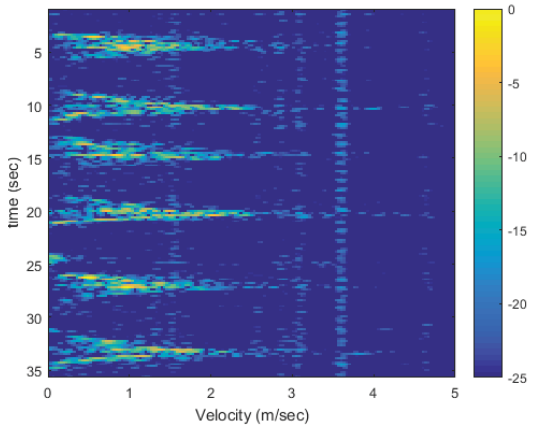

Fig. 14. Doppler measurement data of a running/walking man for velocity (m/s) and received signal amplitude (colorbar in dB) during a through wall experiment.

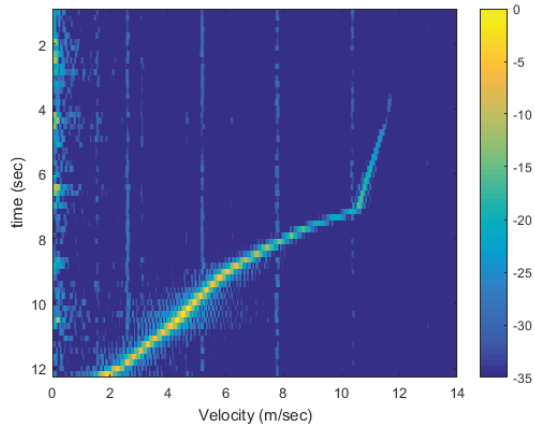

Fig. 15. Doppler measurement data of a car for velocity (m/s) and received signal amplitude (colorbar in dB) in the field experiment.

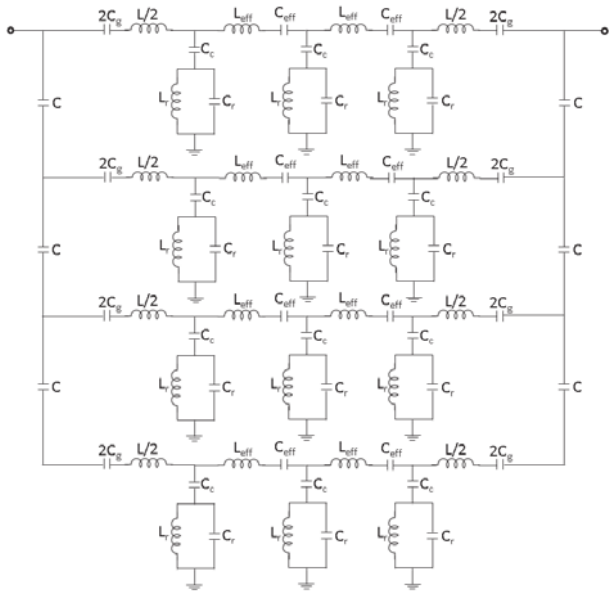

Fig. 16. Simplified equivalent circuit for transmitter antenna.

beamwidth led to localize the angular position of the target, e.g., the received signal is observed when the target movements confine in a certain region. In addition, as a basic result

of the second experiment, one can infer that the proposed system can be employed for velocity measurements of the human targets behind the concrete walls.

V. Conclusion

In this paper, applicability and the effectiveness of the metamaterial-based transmitter and receiver antennas are tested on a short-range and relatively low-cost (<400$) Doppler radar system. Measurement results are presented for indoor and outdoor Doppler radar experiments, Tx-Rx vertical/horizontal radiation patterns, and return loss.

For the transmitter antenna, arrays of CSRR on the top layer and periodically distributed cross-strip line gaps on the bottom layer are used in order to obtain a double negative index structure. According to consistent simulation and measurement results, gain of the Tx is 6.5 dB at 5.8 GHz and it resonates at a large bandwidth, which simplifies the impedance matching. The receiver antenna is considered as a near-zero epsilon metamaterial structure having a gain of 11.3 dB at the desired frequency.

Metamaterial antennas have a strong potential to improve radar characteristics from size reduction and range points of views. Therefore, we encourage to investigate different metamaterial structures for the radar applications due to their unique properties, which can also serve for obtaining a large bandwidth, higher gain, and efficiency as compared to a typical patch antenna. This paper shows the success of the simulations for resembling measurement results for such complicated and small structures which could provide confidence for the new antenna designs to the researchers. For a future study, implementing the range measurement option for the radar and improving the radar software are considered.

Appendix
Simplified Equivalent Circuit Model of the Transmitter Antenna

In Fig. 16, L_r and C_r model coupling between CSRR and bottom line via capacitance C_c. L and C correspond to the line inductance and capacitance of the unit cell, respectively. C and C_g represent the capacitances due to gaps. L_{eff} and C_{eff} are effective element values between the CSRRs. The approximate equivalent circuit is prepared based on the simplified model given in [26].

Acknowledgment

The authors would like to thank the anonymous reviewers of the journal for their constructive remarks and valuable suggestions for improving the quality of this paper. They would also like to thank A. Karatay for providing the microstrip patch array design to compare the performance of their receiver antenna.

References

[1] G. L. Charvat, *Small and Short-Range Radar Systems*. New York, NY, USA: Taylor & Francis, 2014.

[2] S. Guan, J. A. Rice, C. Li, and C. Gu, "Automated DC offset calibration strategy for structural health monitoring based on portable CW radar sensor," *IEEE Trans. Instrum. Meas.*, vol. 63, no. 12, pp. 3111–3118, Dec. 2014.

[3] J. Muñoz-Ferreras, Z. Peng, Y. Tang, R. Gómez-García, D. Liang, and C. Li, "Short-range Doppler-radar signatures from industrial wind turbines: Theory, simulations, and measurements," *IEEE Trans. Instrum. Meas.*, vol. 65, no. 9, pp. 2108–2119, Sep. 2016.

[4] S. M. A. T. Hosseini, and H. Amindavar, "A new Ka-band Doppler radar in robust and precise cardiopulmonary remote sensing," *IEEE Trans. Inst. Meas.*, vol. 66, no. 11, pp. 3012–3022, Nov. 2017.

[5] Y. Zhao and Y. Su, "Cyclostationary phase analysis on micro-Doppler parameters for radar-based small UAVs detection," *IEEE Trans. Inst. Meas.*, vol. 67, no. 9, pp. 2048–2057, Sep. 2018.

[6] R. Garg, P. Bhartia, I. Bahl, and A. Ittipiboon, *Microstrip Antenna Design Handbook*. Norwood, MA, USA: Artech House, 2001.

[7] H. Ö. Yılmaz and F. Yaman, "Meta-material antenna design for 5.8 GHz Doppler radar," in *Proc. 34th Int. Phys. Congr. Turkish Phys. Soc.*, 2018, p. 432.

[8] L. Su, J. Naqui, J. Mata-Contreras, and F. Martín, "Modeling and applications of metamaterial transmission lines loaded with pairs of coupled complementary split-ring resonators (CSRRs)," *IEEE Antennas Wireless Propag. Lett.*, vol. 15, pp. 154–157, 2015.

[9] A. Ali and Z. Hu, "Metamaterial resonator based wave propagation notch for ultrawideband filter applications," *IEEE Antennas Wireless Propag. Lett.*, vol. 7, pp. 210–212, 2008.

[10] W. Withayachumnankul and D. Abbott, "Metamaterials in the terahertz regime," *IEEE Photon. J.*, vol. 1, no. 2, pp. 99–118, Aug. 2009.

[11] A. Ebrahimi, W. Withayachumnankul, S. Al-Sarawi, and D. Abbott, "High-sensitivity metamaterial-inspired sensor for microfluidic dielectric characterization," *IEEE Sensors J.*, vol. 14, no. 5, pp. 1345–1351, May 2014.

[12] S. Enoch, G. Tayeb, P. Sabouroux, N. Guérin, and P. Vincent, "A metamaterial for directive emission," *Phys. Rev. Lett.*, vol. 89, no. 21, Nov. 2002, Art. no. 213902.

[13] J. P. Turpin, Q. Wu, D. H. Werner, B. Martin, M. Bray, and E. Lier, "Low cost and broadband dual-polarization metamaterial lens for directivity enhancement," *IEEE Trans. Antennas Propag.*, vol. 60, no. 12, pp. 5717–5726, Dec. 2012.

[14] D. Ramaccia, F. Scattone, F. Bilotti, and A. Toscano, "Broadband compact horn antennas by using EPS-ENZ metamaterial lens," *IEEE Trans. Antennas Propag.*, vol. 61, no. 6, pp. 2929–2937, Jun. 2013.

[15] Y. Liu, X. Guo, S. Gu, and X. Zhao, "Zero index metamaterial for designing high-gain patch antenna," *Int. J. Antennas Propag.*, vol. 2013 Aug. 2013, Art. no. 215681.

[16] L.-W. Li, Y.-N. Li, T.-S. Yeo, J. R. Mosig, and O. J. F. Martin, "A broadband and high-gain metamaterial microstrip antenna," *Appl. Phys. Lett.*, vol. 96, no. 6, Apr. 2010, Art. no. 164101.

[17] R. Marques, F. Martin, and M. Sorolla, *Metamaterials With Negative Parameters, Theory, Design and Microwave Applications*. Hoboken, NJ, USA: Wiley, 2008.

[18] V. G. Veselago, "The electrodynamics of substances with simulatenously negative values of ϵ and μ," *Sov. Phys. Uspekhi*, vol. 10, no. 4, pp. 509–514, 1968.

[19] J. B. Pendry, A. J. Holden, W. J. Stewart, and I. Youngs, "Extremely low frequency plasmons in metallic mesostructures," *Phys. Rev. Lett.*, vol. 76, no. 25, p. 4773, 1996.

[20] J. B. Pendry, A. J. Holden, D. J. Robbins, and W. J. Stewart, "Magnetism from conductors and enhanced nonlinear phenomena," *IEEE Trans. Microw. Theory Techn.*, vol. 47, no. 11, pp. 2075–2084, Nov. 1999.

[21] D. R. Smith, W. J. Padilla, D. C. Vier, S. C. Nemat-Nasser, and S. Schultz, "Composite medium with simultaneously negative permeability and permittivity," *Phys. Rev. Lett.*, vol. 84, no. 18, p. 4184, May 2000.

[22] C. A. Balanis, *Antenna Theory: Analysis and Design*, 3rd ed. Hoboken, NJ, USA: Wiley, 2005.

[23] F. Falcone *et al.*, "Babinet principle applied to the design of metasurfaces and metamaterials," *Phys. Rev. Lett.*, vol. 93, no. 19, Nov. 2004, Art. no. 197401.

[24] J. D. Baena *et al.*, "Equivalent-circuit models for split-ring resonators and complementary split-ring resonators coupled to planar transmission lines," *IEEE Trans. Microw. Theory Techn.*, vol. 53, no. 4, pp. 1451–1461, Apr. 2005.

[25] G. V. Eleftheriades, A. K. Iyer, and P. C. Kremer, "Planar negative refractive index media using periodically L-C loaded transmission lines," *IEEE Trans. Microw. Theory Techn.*, vol. 50, no. 12, pp. 2702–2712, Dec. 2002.

[26] I. Gil, J. Bonache, M. Gil, J. García-García, F. Martín, and R. Marqués, "Accurate circuit analysis of resonant-type left handed transmission lines with inter-resonator coupling," *J. Appl. Phys.*, vol. 100, no. 7, 2006, Art. no. 074908.

[27] S. S. Islam, M. R. I. Faruque, and M. T. Islam, "The design and analysis of a novel split-H-shaped metamaterial for multi-band microwave applications," *Materials*, vol. 7, no. 7, pp. 4994–5011, 2014.
[28] *CST Microwave Studio*, CST AG-Computer Simulation, Bengaluru, Karnataka, 2016.
[29] J. B. Pendry, "Negative refraction makes a perfect lens," *Phys. Rev. Lett.*, vol. 85, no. 18, p. 3966, Oct. 2000.
[30] D. Schurig *et al.*, "Metamaterial electromagnetic cloak at microwave frequencies," *Sci. Express*, vol. 314, no. 5801, pp. 977–980, Oct. 2006. doi: 10.1126/science.1133628.
[31] D. M. Pozar, *Microwave Engineering*, 4th ed. Hoboken, NJ, USA: Wiley, 2012.
[32] *MIT OpenCourseWare: Build a Small Radar System Capable of Sensing Range, Doppler, and Synthetic Aperture Radar Imaging*. Accessed: May 2017. [Online]. Available: https://ocw.mit.edu
[33] C. Saha and J. Y. Siddiqui, "A comparative analysis for split ring resonators of different geometrical shapes," in *Proc. IEEE Appl. Electromagn. Conf. (AEMC)*, Dec. 2011, pp. 1–4.
[34] A. A. Saleh and A. S. Abdullah, "A novel design of patch antenna loaded with complementary split-ring resonator and L-shape slot for (WiMAX/WLAN) applications," *I.J. Wireless Microw. Technol.*, vol. 3, pp. 16–25, Oct. 2014.
[35] G. Lubkowski, "Simulation of electromagnetic fields in double negative metamaterials," Ph.D. dissertation, Dept. Elect. Eng. Inf. Technol., Darmstadt Tech. Univ., Darmstadt, Germany, 2009.
[36] D. R. Smith, S. Schultz, P. Markos, and C. M. Soukoulis, "Determination of effective permittivity and permeability of metamaterials from reflection and transmission coefficients," *Phys. Rev. B, Condens. Matter*, vol. 65, Apr. 2002, Art. no. 195104.
[37] X. Chen, T. M. Grzegorczyk, B. Wu, J. Pacheco, Jr., and J. A. Kong, "Robust method to retrieve the constitutive effective parameters of metamaterials," *Phys. Rev. E, Stat. Phys. Plasmas Fluids Relat. Interdiscip. Top.*, vol. 70, Jul. 2004, Art. no. 016608.
[38] P. Markoš and C. M. Soukoulis, "Transmission properties and effective electromagnetic parameters of double negative metamaterials," *Opt. Express*, vol. 11, no. 7, pp. 649–661, 2003.
[39] K. C. Teng, "The design and evaluation of a 5.8 GHz laptop-based radar system," M.S. thesis, Graduate School, Purdue Univ., West Lafayette, IN, USA, 2013.
[40] H. Ö. Yılmaz, "Metamaterial antenna design for 5.8 GHz Doppler radar," M.S. thesis, Dept. Electr.-Electron. Eng., Izmir Inst. Technol., Urla, Turkey, 2018.

Hasan Önder Yılmaz was born in Antalya, Turkey, in 1991. He received the B.S. degree in electrical and electronics engineering from Dokuz Eylul University, Izmir, Turkey, in 2014, and the M.S. degree from the Izmir Institute of Technology, Izmir, in 2018, where he is currently pursuing the Ph.D. degree.

He was a Research Assistant with the Electrical and Electronics Engineering Department, Izmir Institute of Technology. His current research interests include optoelectronic, metamaterial applications such as sensors and antennas and microwave engineering.

Fatih Yaman was born in Istanbul, Turkey, in 1978. He received the M.S. degree in electrical and electronics engineering from Istanbul University, Istanbul, in 2004, and the Ph.D. degree in electronics and communication engineering from Istanbul Technical University, Istanbul, in 2009.

From 2001 to 2003, he was a Research Assistant with Istanbul University. From 2005 to 2009, he was a Research Assistant with Istanbul Technical University. From 2006 to 2008, he was a DAAD Scholar with the Institute for Numerical and Applied Mathematics, Georg-August University, Göttingen, Germany. From 2010 to 2014, he was a Post-Doctoral Research Associate with the Institut für Theorie Elektromagnetischer Felder, Technische Universität Darmstadt, Darmstadt, Germany. He is currently an Assistant Professor with the Electrical and Electronics Engineering Department, Izmir Institute of Technology, Izmir, Turkey. His current research interests include direct and inverse problems in acoustic and electromagnetic scattering theory, computational accelerator physics, applied electromagnetics, and Doppler radars.